COMMUNICATION

Direct comparison of covalently-linked dyad and a 1:1 mixture of tetrabenzoporphyrin and fullerene as organic photovoltaic materials

Yuto Tamura,[a] Hiroyuki Saeki,[a] Junpei Hashizume,[b] Yukinori Okazaki,[b] Daiki Kuzuhara,[a] Mitsuharu Suzuki,[a] Naoki Aratani[a] and Hiroko Yamada*[ac]

A p–i–n organic photovoltaic cell with tetrabenzoporphyrin (BP), a BP–C$_{60}$ dyad and PCBM for the p-, i- and n-layers, respectively, gave a better fill factor and power conversion efficiency than a corresponding p–i–n cell having a 1:1 blend film of BP and PCBM as the i-layer.

Solution-processed organic photovoltaic cells (OPVs) have been attracting much attention,[1] and high power conversion efficiencies (PCEs) exceeding 8% have been attained in small-molecular bulk-heterojunction (BHJ) devices.[2] One of the requirements in order to achieve such high PCEs is the balanced formation of large donor–acceptor (D–A) interface and directional charge-carrier paths within the organic active layer; however, it is usually difficult to obtain an ideal film morphology through simple solution-deposition techniques.

D–A dyads have been widely studied to understand charge separation and recombination processes between donor and acceptor units.[3] In addition, various dyad compounds have been examined for use as active materials in BHJ OPVs,[4] since direct connection of donor and acceptor components can be beneficial for forming maximal D–A interface within a film, thereby allowing high charge-separation efficiency. On the other hand, no p–i–n-type device with a D–A dyad has been reported as far as we know, although the employment of the p–i–n structure may lead to enhanced efficiencies.[5]

Tetrabenzoporphyrin (BP) is one of the superior p-type organic semiconductors. Although BP is not soluble in common organic solvents, thin films of BP can be prepared via solution-based deposition techniques by employing a soluble, thermo-labile precursor, bicyclo[2.2.2]octadiene(BCOD)-fused porphyrin (CP).[6] Specifically, a BP film can be prepared by depositing CP by spin-coating then heating the resulting film around 180 ºC to induce the in-situ conversion of CP to BP. This methodology enabled preparation of solution-processed organic field-effect transistors and OPVs based on nano-crystalline BP films.[5,7,8]

With these in mind, we expected that D–A dyads having BP as a donor would allow us to systematically investigate the effect of covalent linkage between donor and acceptor units in solution-processed BHJ or p–i–n devices. In this report, we will present the synthesis of a dyad consisting of BP and C$_{60}$ units (BP–C$_{60}$), as well as its soluble precursor (CP–C$_{60}$). The linker of BP–C$_{60}$ is flexible to ensure the solubility of CP–C$_{60}$ as shown in Fig. 1. We also compare the photovoltaic performances of BP–C$_{60}$ films with those of 1:1 blend films of BP and [6,6]-phenyl-C$_{61}$-butyric acid methyl ester (PCBM) in p–i–n or BHJ OPVs. Here, each p–i–n active layer has a configuration of [BP/BP–C$_{60}$/PCBM] or [BP/BP:PCBM(1:1)/PCBM].

The synthetic route of CP-C$_{60}$ is shown in Scheme S1, ESI†. An acid-catalyzed condensation of BCOD-α-free dipyrrylmethane,[9] n-butanal, and 4-methoxycarbonylbutan-1-al[10] was performed, followed by oxidation with p-chloranil. After insertion of zinc ion, the zinc porphyrin monoester was obtained in 22% yield. Reduction of the monoester to the corresponding alcohol by LiAlH$_4$ (76% yield) and then coupling with [6,6]-phenyl-C$_{61}$-butyric acid[11] (64% yield) gave zinc-CP–C$_{60}$. Zinc-CP–C$_{60}$ was treated with trifluoroacetic acid to afford free-base CP–C$_{60}$ in 86% yield. BuCP was also prepared from BCOD-α-free dipyrrylmethane and n-butanal in 42% yield as a precursor of the reference compound 5,15-dibutylbenzoporphyrin (BuBP). In TGA analyses, weight loss started around 150 ºC and ended around 200 ºC for both CP–C$_{60}$ and BuCP. The decreased weights well correspond to four ethylene units per molecule (Figs. S2 and S4, ESI†).
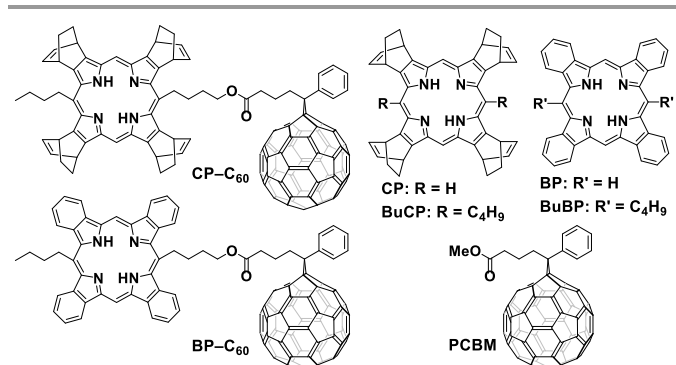
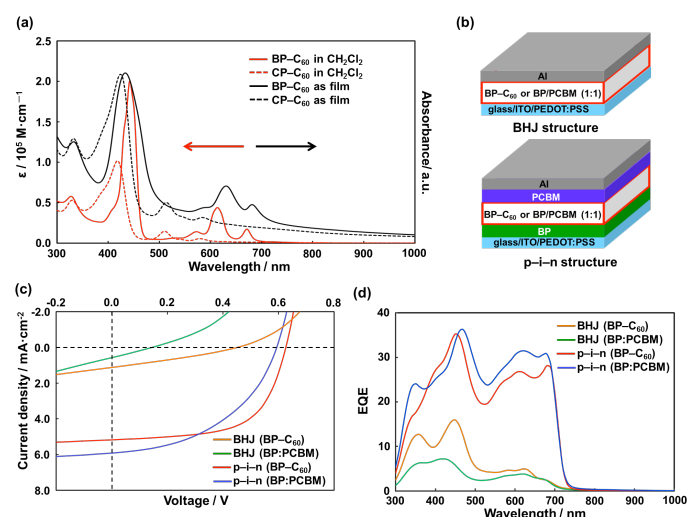Fig. 1 Structures of CP–C$_{60}$, CP, BuCP, BP–C$_{60}$, BP, BuBP and PCBM.

Fig. 2 (a) UV–vis absorption spectra of **CP–C$_{60}$** and **BP–C$_{60}$**. (b) BHJ devices and structures of p–i–n. (c) *J–V* characteristics of the devices. (d) EQE spectra of the devices.

The UV–vis absorption spectra of **CP–C$_{60}$** and **BP–C$_{60}$** in CH$_2$Cl$_2$ are shown in Fig. 2a. The spectrum of **BP–C$_{60}$** has peaks at 442, 573, 614 and 671 nm, which are red-shifted compared to the corresponding peaks of **CP–C$_{60}$** at 420, 512, 542 and 579 nm. The spectrum of **CP–C$_{60}$** is compared to that of a 1:1 mixture of **BuCP** and **PCBM** as shown in Fig. S6, ESI†. The Soret peak of **CP–C$_{60}$** (420 nm) is red-shifted by 10 nm from that of **BuCP** (410 nm) and broadened. The spectrum of **CP–C$_{60}$** does not show the concentration dependency; thus, the intramolecular interaction between the **CP** and **C$_{60}$** units might be the cause of the red-shift and broadening. Similarly, the spectrum of **BP–C$_{60}$** showed the broadening and red-shift of the Soret band compared to the spectrum of a 1:1 mixture of **BuBP** and **PCBM** as shown in Fig. S7, ESI†. Fluorescence of **CP–C$_{60}$** and **BP–C$_{60}$** is quenched drastically compared to **BuCP** and **BuBP** as shown in Fig. S8 and S9, ESI†. The fluorescence quantum yields of **CP–C$_{60}$**, **BuCP**, **BP–C$_{60}$** and **BuBP** were 0.36, 3.1, 1.1 and 11.3%, respectively. This observation again suggests the existence of intramolecular interaction for the dyads in solution, where the **C$_{60}$** moiety can effectively quench the fluorescence from the porphyrin moiety through the photoinduced electron transfer.[3] This interaction must be enabled by the flexibility of the linkage.

The absorption spectra of **CP–C$_{60}$** and **BP–C$_{60}$** films are also shown in Fig. 2a. The film of **BP–C$_{60}$** shows broader peaks compared to those seen in CH$_2$Cl$_2$. The normalized absorption spectrum of **BP–C$_{60}$** film is also compared with those of **BP**, **PCBM**, and the 1:1-blend films (Fig. S10, ESI†). The **BP** film shows a strong Q band at 690 nm, which is typical for crystalline **BP** films.[12] On the other hand, the shape of Q band of **BP–C$_{60}$** film indicates that **BP** units are not effectively stacked to each other within the film. The spectrum of blend film has a larger peak at 690 nm and a broader peak around 640 nm as compared to the **BP–C$_{60}$** film, suggesting partial stacking of **BP** units. The Soret peak of the blend film is also broadened compared to the **BP–C$_{60}$** and **BP** film. The experimentally determined optical band gap (*E$_{gap}$*) and frontier-orbital energies of **BP–C$_{60}$** are summarized in Table S1, ESI†, with those of **BP** and **PCBM** films (Figs. S11 and S12, ESI†). Comparison of these values show that the difference between the LUMO of

PCBM as measured by cyclic voltammetry and HOMO of **BP** as measured by photoemission yield spectroscopy is the same as the HOMO-LUMO difference in the **BP–C$_{60}$** dyad using the same methods to calculate the HOMO and LUMO.

Table 1. Photovoltaic characteristics derived from *J–V* measurements.*

Device	J_{SC}	V_{OC}	FF	PCE	R_s	R_{sh}
	mA cm^{-2}	V		%	Ω cm^2	Ω cm^2
BHJ (**BP–C$_{60}$**)	1.12	0.45	0.29	0.15	163	490
BHJ (**BP:PCBM**)	0.57	0.14	0.23	0.02	219	261
p–i–n (**BP–C$_{60}$**)	5.18	0.62	0.61	1.98	12	1436
p–i–n (**BP:PCBM**)	5.92	0.59	0.46	1.63	16	721

*All values were obtained under AM1.5G illumination at 100 mW cm^{-2}.

Schematic descriptions of the BHJ and p–i–n devices are shown in Fig. 2b. The deposition process of organic active layers is summarized in Fig. S1, ESI† and detailed in the experimental section in ESI†. The BHJ (**BP–C$_{60}$**) device has a **BP–C$_{60}$** active layer, which was prepared by spin-coating of a **CP–C$_{60}$** solution followed by heating at 160 ºC for 20 min. BHJ (**BP:PCBM**) has a 1:1 blend film of **BP** and **PCBM** deposited similarly from a mixed solution of **CP** and **PCBM**. The p–i–n (**BP–C$_{60}$**) film was prepared by sequential deposition of **BP**, **BP–C$_{60}$** and **PCBM** as p-, i-, and n-layers, respectively. The p–i–n (**BP:PCBM**) device has a 1:1 mixture film of **BP** and **PCBM** in the i-layer instead of **BP–C$_{60}$**.

The *J–V* characteristics of the devices are shown in Fig. 2c, and the device performances are summarized in Table 1. The dark currents are plotted in Fig. S13, ESI†. The BHJ (**BP–C$_{60}$**) device showed a better performance (PCE = 0.15%) with a short circuit current density (*J$_{SC}$*) of 1.12 mA cm^{-2}, an open circuit voltage (*V$_{OC}$*) of 0.45 V and a fill factor (FF) of 0.29 than the BHJ (**BP:PCBM**) device (*J$_{SC}$* = 0.57 mA cm^{-2}, *V$_{OC}$* = 0.14 V, FF = 0.23, PCE = 0.02%). Although the BHJ (**BP–C$_{60}$**) device is better than the BHJ (**BP:PCBM**), the dark *J–V* characteristics of both devices show current leakage (Fig. S13). The performance of p–i–n (**BP–C$_{60}$**) and p–i–n (**BP:PCBM**) is much improved; *J$_{SC}$* = 5.18 mA cm^{-2}, *V$_{OC}$* = 0.62 V, FF = 0.61 and PCE = 1.98% for p–i–n (**BP–C$_{60}$**) and *J$_{SC}$* = 5.92 mA cm^{-2}, *V$_{OC}$* = 0.59 V, FF = 0.46, and PCE =1.63% for p–i–n (**BP:PCBM**). The highest FF of p–i–n (**BP–C$_{60}$**) is associated with the lowest series resistance (*R$_s$*) and the highest shunt resistance (*R$_{sh}$*), which suggests the best semiconducting property of the p–i–n (**BP–C$_{60}$**) device among those examined here. Fig. 2d shows external quantum efficiency (EQE) spectra of the devices. The better EQE of BHJ (**BP–C$_{60}$**) than BHJ (**BP:C$_{60}$**) suggests that the carrier generation in the dyad film is more effective than in BHJ (**BP:PCBM**). The spectrum of BHJ (**BP–C$_{60}$**) shows two peaks at 350 and 440 nm corresponding to **C$_{60}$** and **BP**, respectively, which indicates that both units work as sensitizers. The broader, less defined peaks in the EQE spectrum of BHJ (**BP:PCBM**) could be attributed to the stacking of **BP** molecules in the blend films—similar tendency was observed between the UV–vis absorption spectra of these films (Fig. S10, ESI†). The EQEs of the p–i–n (**BP–C$_{60}$**) and p–i–n (**BP:PCBM**) are much enhanced as compared to the BHJ devices. The peak at 350 nm for p–i–n (**BP–C$_{60}$**) is lower than that for p–i–n (**BP:PCBM**), thus the C$_{60}$ moieties do not work effectively as sensitizer in the former device. This seems reflecting the relatively low absorption at this wavelength in the film of **BP–C$_{60}$** (Fig. S10, ESI†), although the reason for the low absorptivity is not clear at this moment.
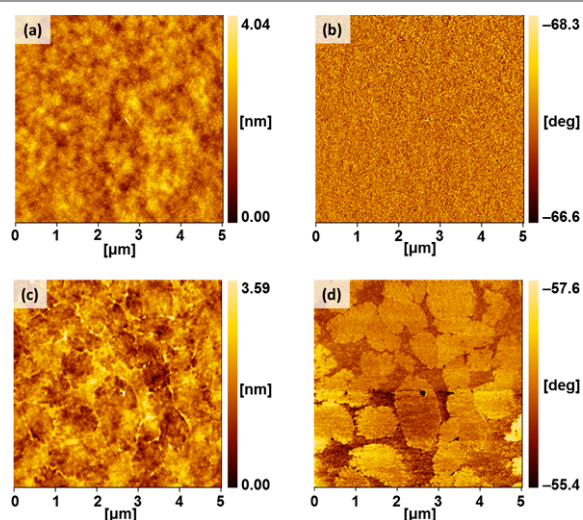
Fig. 3 Tapping–mode AFM height (left) and phase (right) images. (a, b) **BP–C$_{60}$** film; (c,d) blend film of **BP** and **PCBM**.

The tapping–mode atomic force microscopy (AFM) height and phase images of a **BP–C$_{60}$** film and a 1:1 blend film of **BP** and **PCBM** are shown in Fig. 3. The two films are similar in surface roughness, with the RMS values of 0.43 and 0.50 nm for the dyad and blend films, respectively. On the other hand, the phase images showed obvious difference: the dyad film has the smooth surface, but the blend film shows large grains of 1–2 μm diameters. In addition, a dyad film formed on a **BP** layer showed much smoother surface with fewer grains as compared to a corresponding blend film on **BP** (Figs. S14 and S15). Thus, the covalent linkage between the **BP** and **C$_{60}$** units prevents the formation of grains, which may have led to the improvement of the FF. The out-of-plane XRD patterns, on the other hand, did not show the specific peaks for both of the dyad and blend films as shown in Fig. S16, ESI†. The crystallinity of **BP** and **PCBM** in these films seems not so high, although the large grains are observed by AFM phase image of p–i–n (**BP**:**PCBM**) and the Q band of the blend film suggested the partial π–π interaction of **BP** in the blend film.

In summary, we were successful to construct the p–i–n OPV device composed of **BP**, **BP–C$_{60}$**, and **PCBM** for p-, i-, and n-layers, respectively, using the in-situ thermal conversion from solution-deposited **CP** and **CP–C$_{60}$** to insoluble **BP** and **BP–C$_{60}$**. The **BP–C$_{60}$** film showed better performance in a p–i–n device associated with a higher FF compared to the 1:1 blend film of **BP** and **PCBM**. The grain boundaries in the blend film could have increased the resistance in the film and therefore lowered the FF values. On the contrary, the **BP–C$_{60}$** dyad did not form grains and the resultant p–i–n device showed a lower series resistances than the corresponding device based on the blend film. In order to further improve the OPV performance with D–A dyads, higher J_{SC} values should be attained through the improvement of electron-transfer efficiency and the suppression of charge recombination. Synthesis of D–A compounds of the next generation is underway.

Notes and references

^{a}Graduate School of Materials Science, Nara Institute of Science and Technology (NAIST), 8916-5 Takayama-cho, Ikoma 630-0192, Japan, E-mail: hyamada@ms.naist.jp, Fax: +81-743-72-6041; ^{b}Graduate School of Science and Engineering, Ehime University, 2-5 Bunkyo-cho, Matsuyama, 790-8577, Japan; ^{c}CREST, Japan Science and Technology (JST), 4-1-8 Honcho, Kawaguchi, Saitama 332-0012, Japan.

Electronic Supplementary Information (ESI) available: [Synthetic details, device fabrication, absorption and fluorescence spectra, cyclic voltammograms, ionization potentials, *J-V* characteristics, and XRD patterns]. See DOI: 10.1039/c000000x/

1 (*a*) C. J. Brabec, N. S. Sariciftci and J. C. Hummelen, *Adv. Funct. Mater.* 2001, **11**, 15; (*b*) K. M. Coakley and M. D. McGehee, *Chem. Mater.* 2004, **16**, 4533; (*c*) P. M. Beaujuge and J. M. J. Fréchet, *J. Am. Chem. Soc.* 2011, **133**, 20009; (*d*) M. Kaltenbrunner, M. S. White, E. D. Głowacki, T. Sekitani, T. Someya, N. S. Sariciftci and S. Bauer, *Nat. Commun.*, 2012, **3**, 770.

2 (*a*) B. Walker, A. B. Tamayo, X.-D. Dang, P. Zalar, J. H. Seo, A. Garcia, M. Tantiwiwat and T.-Q. Nguyen, *Adv. Funct. Mater.* 2009, **19**, 3063; (*b*) J. Roncali, *Acc. Chem. Res.* 2009, **42**, 1719; (*c*) B. Walker, C. Kim and T.-Q. Nguyen, *Chem. Mater.*, 2011, **23**, 470; (*d*) A. Mishra and P. Bäuerle, *Angew. Chem. Int. Ed.*, 2012, **51**, 2020.

3 (*a*) D. Gust, T. A. Moore and A. L. Moore, *Acc. Chem. Res.* 1993, **26**, 198; (*b*) M. R. Wasielewski, *Chem. Rev.* 1992, **92**, 435; (*c*) A. Osuka, N. Mataga and T. Okada, *Pure Appl. Chem.* 1997, **69**, 797; (*d*) H. Imahori and Y. Sakata, *Adv. Mater.* 1997, **9**, 537; (*e*) S. Fukuzumi and H. Imahori, *In Electron Transfer in Chemistry*; V. Balzani, Ed. Wiley-VCH: Weinheim, Germany, 2001; Vol. 2, pp 927.

4 (*a*) J. L. Segura, N. Martin and D. M. Guldi, *Chem. Soc. Rev.*, 2005, **34**, 31; (*b*) M. Wang and F. Wudl, *J. Mater. Chem.*, 2012, **22**, 24297; (*c*) H. Imahori, T. Umeyama, K. Kurotobi and Y. Takano, *Chem. Commun.*, 2012, **48**, 4032

5 Y. Matsuo, Y. Sato, T. Niinomi, I. Soga, H. Tanaka and E. Nakamura, *J. Am. Chem. Soc.* 2009, **131**, 16048.

6 S. Ito, T. Murashima, H. Uno and N. Ono, *Chem. Commun.,* **1998**, 1661.

7 (*a*) H. Yamada, T. Okujima and N. Ono, *Chem. Commun.,* **2008**, 2957; (*b*) H. Saeki, M. Misaki D. Kuzuhara, H. Yamada and Y. Ueda, *Jpn. J. Appl. Phys.* 2013, **52**, 111601; (*c*) H. Saeki, O. Kurimoto, M. Misaki, D. Kuzuhara, H. Yamada and Y. Ueda, *Appl. Phys. Express.*, 2013, **6**, 035601.

8 M. Guide, X.-D. Dang and T.-Q. Nguyen, *Adv. Mater.*, 2011, **23**, 2313.

9 H. Yamada, K. Kushibe, T. Okujima, H. Uno and N. Ono, *Chem Commun.*, 2006, 383.

10 V. Hickmann, A. Kondoh, B. Gabor, M. Alcarazo and A. Fürstner, *J. Am. Chem. Soc.* 2011, **133**, 13471.

11 T. Nishizawa, K. Tajima and K. Hashimoto, *J. Mater. Chem.*, 2007, **17**, 2440.

12 C. D. Liman, S. Choi, D. W. Breiby, J. E. Cochran, M. F. Toney, E. J. Kramer and M. L. Chabinyc, *J. Phys. Chem. B*, 2013, **117**, 14557.

GA
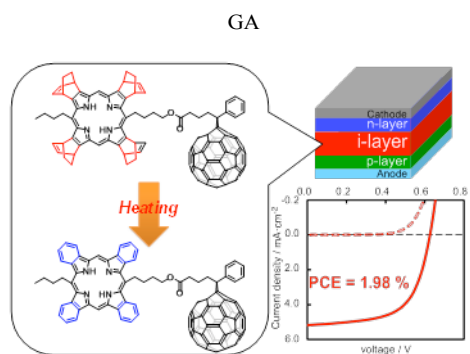
Effective covalent linkage of tetrabenzorporphyrin and fullerene for i-layer of p–i–n OPVs with FF of 0.61 and PCE of 1.98%